Mon. Not. R. Astron. Soc. **000**, 1–6 (2015) Printed 21 July 2015 (MN LATEX style file v2.2)

Filling in the 2MASX Redshift in the southern Zone of Avoidance using 21 cm HI emission line

K. Said[1,2,3⋆], R. C. Kraan-Korteweg[1], L. Staveley-Smith[2,3], T. H. Jarrett[1], A. C. Schröder[4], P. A. Henning[5], and W. van Driel[6]

[1]*Astrophysics, Cosmology and Gravity Centre (ACGC), Astronomy Department, University of Cape Town, Private Bag X3, Rondebosch, 7701, South Africa*
[2]*ICRAR, M468, The University of Western Australia, 35 Stirling Highway, Crawley, WA 6009, Australia*
[3]*ARC Centre of Excellence for All-sky Astrophysics (CAASTRO)*
[4]*South African Astronomical Observatory, P.O. Box 9 Observatory 7935, Cape Town, South Africa*
[5]*Department of Physics and Astronomy, University of New Mexico, Albuquerque, NM 87131, USA*
[6]*GEPI, Observatoire de Paris, CNRS, Université Paris Diderot, 5 place Jules Janssen, 92190 Meudon, France*

Accepted 00. Received 00; in original form 00

ABSTRACT

Unveil the redshift of nearby galaxies behind the Milky Way may affect the direction of the local group dipole and solve the discrepancy with the direction of the CMB dipole. Dust extinction and stellar confusion are the main limitations of the optical spectroscopy. Indeed, 21-cm observations have opened an elegant way to complement the redshift and peculiar velocity surveys at low galactic latitude because 21-cm emission line does not suffer from foreground dust extinction. We obtain 21 cm HI emission line profiles for 246 bright 2MASX galaxies in the southern zone of avoidance that have no previous redshift measurement and were excluded from the current most homogeneous all-sky redshift survey, 2MASX Redshift Survey. Observations were conducted in 2013 and 2014 with the multibeam receiver, its high-efficiency 7 inner beams, on the Parkes 64m radio telescope. We reached an rms of 3mJy for our spectra which is consistent with Nançay radio telescope observations in the northern sky and a factor of two lower than the HIZoA original catalog. This resulted in 40 HI new detection. The relatively low detection rate can be understood; given that this same area have been surveyed twice in both HIPASS and HIZoA. These new HI profiles will be used in the future to complement the 2MASS Redshift survey and 2MASS Tully-Fisher survey.

Key words: galaxies: spiral – galaxies: distances and redshifts – radio lines: galaxies – infrared: galaxies – cosmology: observations – cosmology: large-scale structure of Universe

1 INTRODUCTION

Mapping the distribution of nearby galaxies in three-dimensional is not only useful for cosmography; but also for dynamical studies of the local universe. The observed dipole anisotropy in the Cosmic Microwave Background (CMB) usually interpreted as a direct result from the Doppler shift of the Local Group (LG) velocity of $v_{LG} = 627 \pm 22$km s^{-1} toward $(l, b) = (276 \pm 3^\circ, 30 \pm 2^\circ)$ (Kogut et al. 1993). Between the mid 1980s and the early 2000s, many measurements of the gravitational dipole from different redshift surveys obtain controversial results compared to the CMB dipole (Strauss & Willick 1995; Schmoldt et al. 1999), and references therein). One of the proposed origin of this discrepancy is that, non of the existing redshift surveys at that time cover the whole-sky because of the dust extinction and stellar density at low galactic latitude, the so-called Zone of Avoidance (ZoA) (Kraan-Korteweg & Lahav 2000).

Today, with the existence of the 2MASS Redshift Survey (2MRS; Huchra et al. 2012), the situation has partly improved. The 2MRS is based on the 2MASS extended source catalog (2MASX; Jarrett et al. 2000; Jarrett 2004) and mostly complete to $K_s = 11.75$ mag and $|b| \geqslant 5^\circ$ ($\geqslant 8^\circ$ toward the Galactic bulge). Earlier version of the 2MRS catalog (Huchra et al. 2005) have been used in several dynamical studies (Erdoğdu et al. 2006a,b; Loeb & Narayan 2008; Erdoğdu & Lahav 2009; Lavaux et al. 2010; Davis et al. 2011; Bilicki et al. 2011). These studies were still limited to statistical interpolations because of the so-called NIR ZoA ($|b| \geqslant 5^\circ$ and $\geqslant 8^\circ$ toward the Galactic bulge). Our goal in this paper is to probe deeper into the ZoA and provide a redshift for all galaxies that were excluded from the 2MRS.

The only path for covering the most obscured regions in the ZoA is through HI observations. The Milky-Way is almost transparent to these kind of observations that are designed to detect the 21-cm emission line in galaxies confusion, such as HIPASS for the

⋆ E-mail: khaled@ast.uct.ac.za

southern sky (Koribalski et al. 2004) and the EBHIS for the northern sky (Kerp et al. 2011).

The HI Parkes Deep Zone of Avoidance Survey (HIZoA) in the southern ZoA ($|b| < 5^\circ$; Dec $< +15^\circ$) was performed in parallel with the HIPASS survey, but has 5-times longer integration time, and resulted in more than a thousand detected galaxies with rms $\sim$ 6mJy/beam (Kraan-Korteweg et al. 2005; Donley et al. 2005, Henning et al. in prep, Kraan-Korteweg et al. in prep). Unfortunately, no similar systematic survey is presently in existence in the northern sky. Selected regions of the northern ZoA have been observed with the Arecibo (Springob et al. 2008; Henning et al. 2008, 2010). Subsequently, pointed HI observations of optical selected galaxies have been made in both southern and northern skies and revealed many structures hidden behind the Milky Way (Kraan-Korteweg et al. 1996, 2002; Schröder et al. 2009).

In 2009, an observing programme have been started to obtain HI redshift for 2MASX selected galaxies, $K_s^o < 11.25$ mag and $|b| < 10^\circ$, without previous redshift to fill the gap in the 2MRS (van Driel et al. 2009). A thousand galaxies without previous redshift measurement and Dec $> -38^\circ$ have been observed to an rms $\sim$ 3 mJy/beam and $v \lesssim 10500$ km s^{-1} with the Nançay Radio Telescope. This resulted in over 250 new HI detection. In 2013, we start using the Parkes 64m radio telescope to complete the survey and cover the southern part of the ZoA. 246 bright 2MASX galaxies without redshift in the southern ZoA have been observed to to an rms $\sim$ 3mJy/beam which is consistent with the observations in the northern ZoA. This resulted in 40 new HI detection.

These data provides a unique cover of the whole ZoA from the northern to southern end and complement the 2MRS to the most obscured regions. Some of these data will also be used to measure the real distances and peculiar velocity in the ZoA (Said et al. 2014, 2015). This will complement the 2MASS Tully-Fisher (T-F) survey (Masters et al. 2008; Hong et al. 2013; Masters et al. 2014; Hong et al. 2014; Springob et al. 2015) and results in the most complete T-F survey.

Outline

2 OBSERVATIONS AND DATA REDUCTION

2.1 Sample Selection

We first identified all 2MASX galaxy candidates brighter than the extinction-corrected magnitude $K_s^o = 11\overset{\text{m}}{.}25$ without previous redshift measurements in the ZoA ($|b| < 10^\circ$). Based on our experience with the NRT pilot survey (van Driel et al. 2009), we selected the galaxy candidates through careful scrutiny of all the sources on NIR and optical images and rejection of sources with improbable extinction-corrected NIR colours for galaxies. This galaxy list was cross-correlated with the literature to exclude the ones which have published redshifts. We also verified that they were not recovered in either the (unpublished) Parkes deep HIZOA survey (Kraan-Korteweg, priv. comm), the Arecibo shallow ZoA survey (Henning, priv. comm.) or unpublished 2MRS data (Macri, priv. comm.).

2.2 Data Acquisition

Data were collected in 2013 and 2014 using the 64 m Parkes Radio Telescope with the Multibeam receiver (Staveley-Smith et al. 1996). Using the 7 high-efficiency inner beams in the beam-switching mode allows one beam ON the source and the other six OFF source which reduces the noise by a factor of $\sqrt{6}$. To be consistent with the NRT observations in the northern sky, we require an rms of 3mJy, a factor of two lower than the HIZoA original catalog, for our spectra. This was achieved with 35 minutes of on-source integration, assuming 64 MHz bandwidth split into 1024 channels. With the total allocated time of 216 hours, 246 2MASX galaxies without previous redshift measurements in the ZoA have been observed with a velocity resolution of 14 km s^{-1} which is sufficient for redshift determinations.

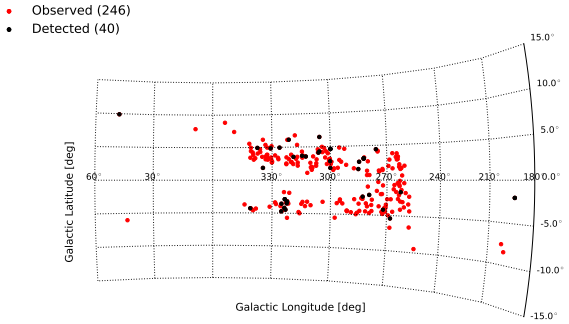

Figure 1. The distribution of all 246 2MASX bright galaxies without redshift determinations in the southern ZoA (Red-dots). Black-dots shows the preliminary list of the HI detection.

2.3 Data Reduction

Preliminary processing of the data was done in the real time of observation. Each galaxy was observed with 35 minutes. To avoid the Global position System (GPS), this integration time for all sources were reduced to 2 $\times$ 17.5 minutes. Based on this preliminary results, some galaxies were observed for further 17.5 or even 35 minutes. We used the package **LIVEDATA**[1] (Barnes et al. 2001) to correct for the bandpass and Doppler effects. Estimation of the bandpass is done by using the MEDIAN estimator instead of the MEAN estimator. All spectra were converted to the Solar System barycentre. The corrected-spectra were gridded with **GRIDZILLA**[2] (Barnes et al. 2001) using the MEDIAN algorithm.

3 HI RESULTS

246 bright 2MASX galaxies without redshift in the southern ZoA have been observed to to an rms $\sim$ 3mJy/beam; this resulted in a preliminary list of 40 new HI detection. This preliminary list of the HI detection was completed in the real time of observations by me. Figure 1 shows the distribution of the 264 2MASX bright galaxies

[1] This software is available in the ATNF package of AIPS++
[2] This software is available in the ATNF package of AIPS++

and the 40 HI detection.

3.1 Galactic HI and False-Detection

I adjust the velocity limit to be from 250 to 12500 km s^{-1} to avoid the Galactic HI. I also excluded all candidates with velocity widths < 25 km s^{-1} to avoid false detection from Radio Frequency Interference (RFI) and hydrogen recombination lines. This resulted in excluding 4 of the preliminary detection. Names and parameters of the false detection are summarized in Table 1 and Fig. 2.

REFERENCES

Barnes D. G. et al., 2001, MNRAS, 322, 486
Bilicki M., Chodorowski M., Jarrett T., Mamon G. A., 2011, ApJ, 741, 31
Davis M., Nusser A., Masters K. L., Springob C., Huchra J. P., Lemson G., 2011, MNRAS, 413, 2906
Donley J. L. et al., 2005, AJ, 129, 220
Erdoğdu P. et al., 2006a, MNRAS, 368, 1515
Erdoğdu P., Lahav O., 2009, Phys. Rev. D, 80, 043005
Erdoğdu P. et al., 2006b, MNRAS, 373, 45
Henning P. A. et al., 2008, in Minchin R., Momjian E., eds, American Institute of Physics Conference Series Vol. 1035, The Evolution of Galaxies Through the Neutral Hydrogen Window. pp 246–248
Henning P. A. et al., 2010, AJ, 139, 2130
Hong T. et al., 2014, MNRAS, 445, 402
Hong T. et al., 2013, MNRAS, 432, 1178
Huchra J. et al., 2005, in Fairall A. P., Woudt P. A., eds, Astronomical Society of the Pacific Conference Series Vol. 329, Nearby Large-Scale Structures and the Zone of Avoidance. p. 135
Huchra J. P. et al., 2012, ApJS, 199, 26
Jarrett T., 2004, Publ. Astron. Soc. Aust., 21, 396
Jarrett T. H., Chester T., Cutri R., Schneider S., Skrutskie M., Huchra J. P., 2000, AJ, 119, 2498
Kerp J., Winkel B., Ben Bekhti N., Flöer L., Kalberla P. M. W., 2011, Astronomische Nachrichten, 332, 637
Kogut A. et al., 1993, ApJ, 419, 1
Koribalski B. S. et al., 2004, AJ, 128, 16
Kraan-Korteweg R. C., Henning P. A., Schröder A. C., 2002, A&A, 391, 887
Kraan-Korteweg R. C., Lahav O., 2000, A&A Rev., 10, 211
Kraan-Korteweg R. C., Staveley-Smith L., Donley J., Koribalski B., Henning P. A., 2005, in Colless M., Staveley-Smith L., Stathakis R. A., eds, IAU Symposium Vol. 216, Maps of the Cosmos. p. 203
Kraan-Korteweg R. C., Woudt P. A., Cayatte V., Fairall A. P., Balkowski C., Henning P. A., 1996, Nature, 379, 519
Lavaux G., Tully R. B., Mohayaee R., Colombi S., 2010, ApJ, 709, 483
Loeb A., Narayan R., 2008, MNRAS, 386, 2221
Masters K. L., Crook A., Hong T., Jarrett T. H., Koribalski B. S., Macri L., Springob C. M., Staveley-Smith L., 2014, MNRAS, 443, 1044
Masters K. L., Springob C. M., Huchra J. P., 2008, AJ, 135, 1738
Said K., Kraan-Korteweg R. C., Jarrett T. H., 2014, preprint (astro-ph/1410.2992)
Said K., Kraan-Korteweg R. C., Jarrett T. H., 2015, MNRAS, 447, 1618
Schmoldt I. et al., 1999, MNRAS, 304, 893
Schröder A. C., Kraan-Korteweg R. C., Henning P. A., 2009, A&A, 505, 1049
Springob C. M. et al., 2008, in Davies J. I., Disney M. J., eds, IAU Symposium Vol. 244, IAU Symposium. pp 383–384
Springob C. M. et al., 2015, in American Astronomical Society Meeting Abstracts. p. 419.04
Staveley-Smith L. et al., 1996, Publ. Astron. Soc. Aust., 13, 243
Strauss M. A., Willick J. A., 1995, Phys. Rep., 261, 271
van Driel W., Schneider S. E., Kraan-Korteweg R. C., Monnier Ragaigne D., 2009, A&A, 505, 29

This paper has been typeset from a TEX/ LATEX file prepared by the author.

Table 1. Parameters of Parkes False detection

Name	l	b	v_m [km/s]	v50 [km/s]	v20 [km/s]	w50	w20	Flux [Jy km/s]	rms [mJy]	S/N
2MASXJ06074754+1604526b	193.683	-2.038	9842	9841	9841	14	21	1.18	3.2	25.35
2MASXJ10075027-5848089	283.089	-2.384	4368	4368	4368	14	23	0.57	3.6	11.41
2MASXJ12285595-5805496c	299.952	4.644	9908	9913	9905	19	96	1.15	2.8	10.10
2MASXJ15252022-5050384	326.156	4.955	4394	4387	4392	17	33	0.54	3.1	8.85

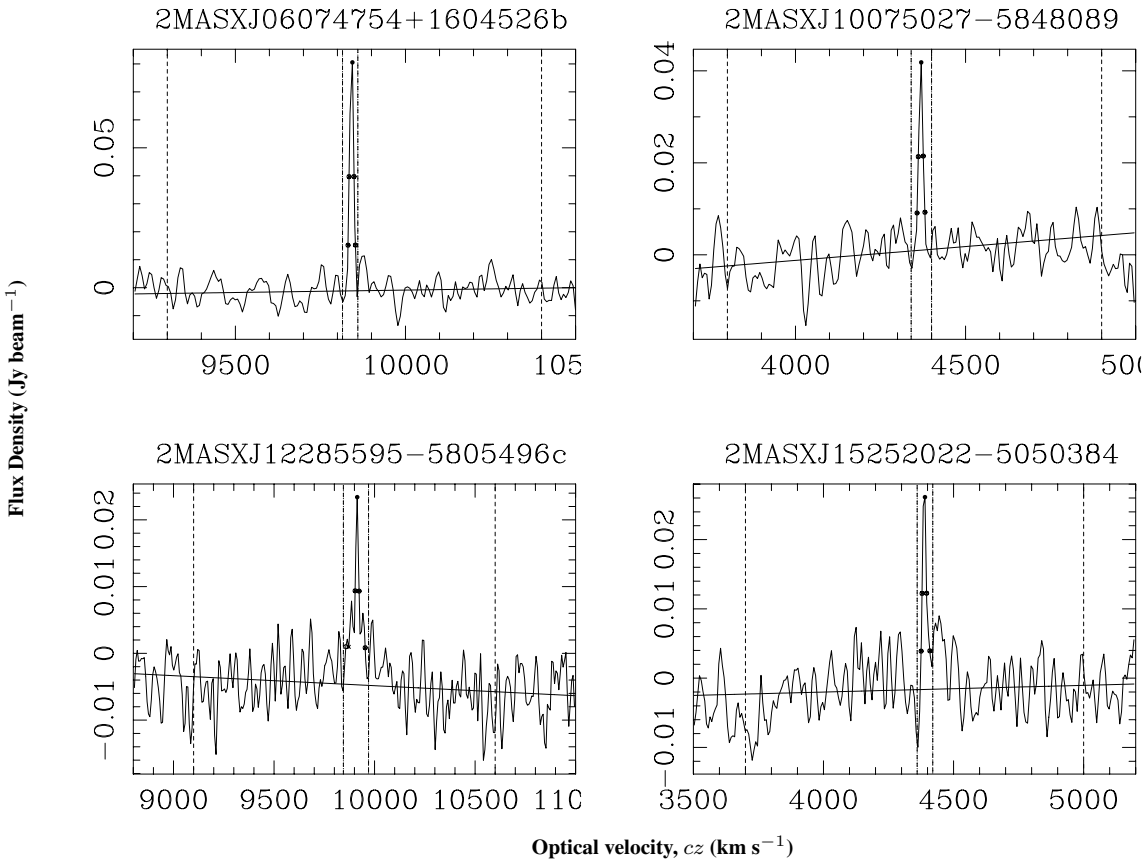

Figure 2. Spectra of Parkes false detection

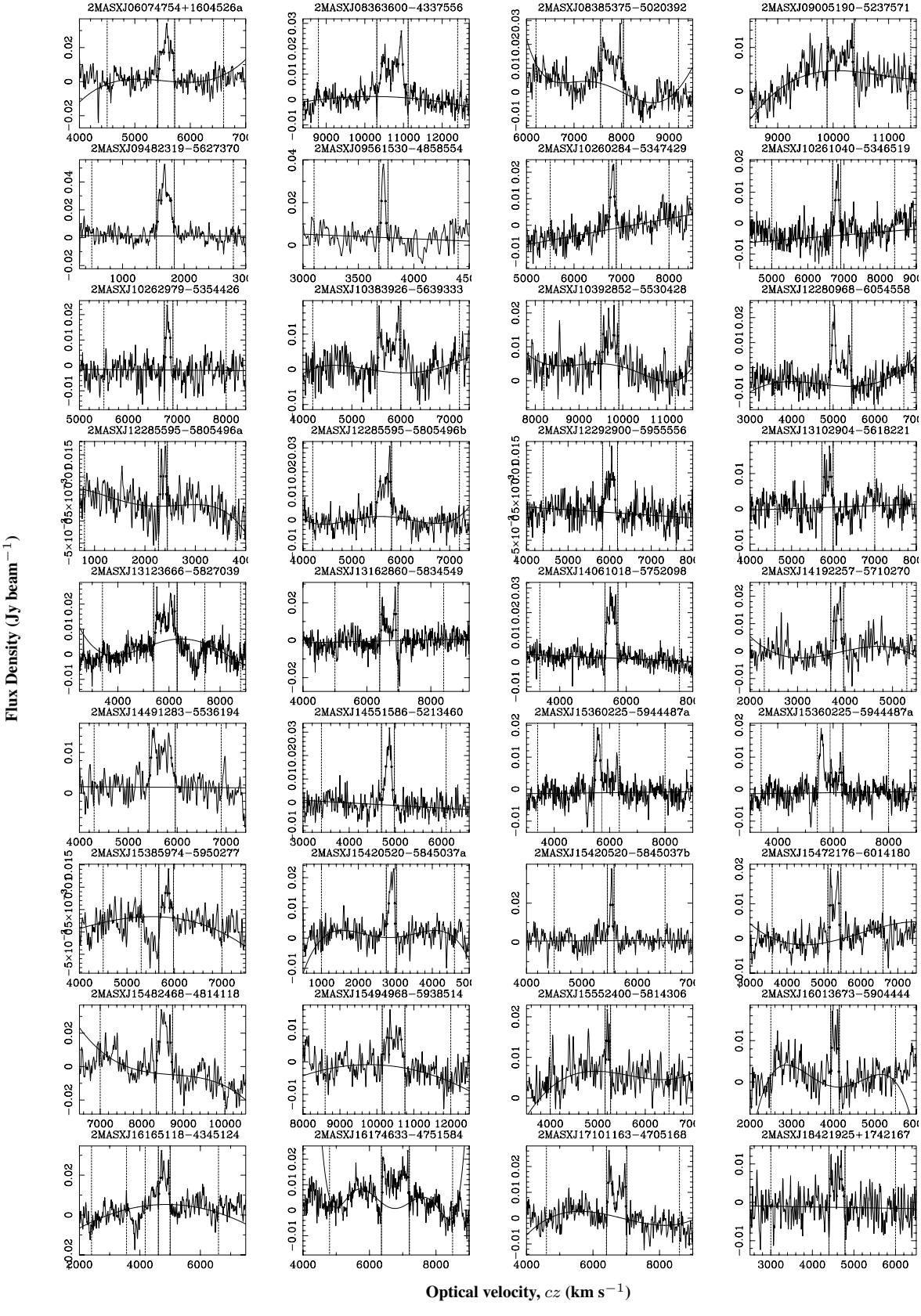

Figure 3. Spectra of Parkes detection

Table 2. Parkes detection.

Name	l	b	v_m [km/s]	v50 [km/s]	v20 [km/s]	w50	w20	Flux [Jy km/s]	rms [mJy]	S/N
2MASXJ06074754+1604526a	193.683	-2.038	5570	5571	5568	238	263	5.27	3.6	9.28
2MASXJ08363600-4337556	262.451	-1.681	10722	10706	10722	552	689	8.31	2.2	12.12
2MASXJ08385375-5020392	268.052	-5.417	7797	7789	7806	394	443	5.63	3.5	8.15
2MASXJ09005190-5237571	271.997	-4.204	10152	10127	10128	443	450	1.59	2.0	5.57
2MASXJ09482319-5627370	279.596	-2.121	1687	1685	1695	207	255	7.70	3.4	14.88
2MASXJ09561530-4858554	275.829	4.449	3727	3725	3726	36	50	1.18	3.7	9.15
2MASXJ10260284-5347429	282.407	3.180	6813	6807	6811	87	134	2.15	2.7	8.85
2MASXJ10261040-5346519	282.415	3.202	6806	6808	6794	92	176	2.02	2.4	9.59
2MASXJ10262979-5354426	282.525	3.116	6807	6810	6809	92	111	1.64	3.0	8.46
2MASXJ10383926-5639333	285.412	1.627	5778	5761	5760	433	446	3.98	2.9	6.52
2MASXJ10392852-5530428	284.954	2.685	9706	9718	9715	337	350	2.70	3.3	7.08
2MASXJ12280968-6054558	300.106	1.828	5150	5178	5180	418	497	5.84	2.7	11.93
2MASXJ12285595-5805496a	299.952	4.644	2377	2367	2364	111	125	0.93	2.3	5.89
2MASXJ12285595-5805496b	299.952	4.644	5675	5682	5652	217	292	4.00	2.4	12.22
2MASXJ12292900-5955556	300.182	2.822	6010	6020	5999	202	271	1.82	1.8	8.04
2MASXJ13102904-5618221	305.588	6.467	5870	5863	5875	171	221	1.95	2.5	6.96
2MASXJ13123666-5827039	305.707	4.307	5856	5867	5845	708	763	7.64	2.3	9.62
2MASXJ13162860-5834549	306.199	4.131	6648	6678	6675	444	461	3.99	3.2	8.79
2MASXJ14061018-5752098	312.76	3.569	5556	5556	5553	291	330	6.16	1.9	14.85
2MASXJ14192257-5710270	314.665	3.681	3851	3838	3842	156	201	2.57	2.5	9.46
2MASXJ14491283-5536194	319.085	3.529	5678	5671	5693	416	502	4.33	1.9	7.52
2MASXJ14551586-5213460	321.407	6.144	4850	4858	4842	121	196	3.79	2.9	11.50
2MASXJ15360225-5944487a	322.326	-3.224	5784	5571	5585	178	231	3.13	1.9	10.45
2MASXJ15360225-5944487b	322.326	-3.224	6118	6102	6105	382	399	2.06	1.9	6.46
2MASXJ15385974-5950277	322.57	-3.52	5858	5848	5840	81	229	0.94	1.7	6.25
2MASXJ15420520-5845037a	323.541	-2.884	2894	2905	2884	162	223	3.48	1.9	12.13
2MASXJ15420520-5845037b	323.541	-2.884	5528	5532	5522	40	79	1.74	3.1	12.02
2MASXJ15472176-6014180	323.16	-4.47	5299	5286	5290	244	263	3.17	1.8	11.40
2MASXJ15482468-4814118	330.732	4.85	8542	8546	8542	295	363	8.81	4.9	7.86
2MASXJ15494968-5938514	323.771	-4.201	10455	10463	10450	392	566	4.47	2.4	7.12
2MASXJ15552400-5814306	325.222	-3.569	5209	5215	5211	64	83	0.75	2.5	6.09
2MASXJ16013673-5904444	325.291	-4.731	4043	4047	4045	162	179	2.28	2.4	7.68
2MASXJ16165118-4345124	337.421	4.941	4794	4821	4800	278	341	5.17	3.5	7.79
2MASXJ16174633-4751584	334.662	1.882	6784	6776	6777	772	786	8.89	2.6	8.08
2MASXJ17101163-4705168	341.047	-4.295	6705	6719	6710	516	552	6.02	2.4	10.26
2MASXJ18421925+1742167	47.838	9.927	4595	4570	4591	273	337	2.30	2.8	5.21